EXPERIMENTAL CYCLIC BEHAVIOR OF HOLLOW-SECTION BRIDGE PIERS WITH DIFFERENT TRANSVERSE REINFORCEMENT DETAILS

P. Delgado[1], N. Vila-Pouca[2], A. Arêde[2], P. Rocha[1], A. Costa[3] and R. Delgado[2]

[1] *Polytechnic Institute, Viana do Castelo, Portugal*
[2] *Faculty of Engineering of the University of Porto, Portugal*
[3] *University of Aveiro, Portugal*
Email: pdelgado@estg.ipvc.pt, pdelgado@fe.up.pt

ABSTRACT :

The main purpose of this paper is to present an experimental and numerical study concerning the influence of the transverse reinforcement details on the cyclic behavior of RC hollow bridge piers. Another strong motivation for this work relies on the fact that rectangular RC hollow piers exhibit a peculiar structural behavior, close to structural wall, and therefore it is more difficult to assess their cyclic response with simple numerical tools. Being representative of typical bridge construction, several RC piers were tested at LESE – FEUP (Laboratory for Earthquake and Structural Engineering of the Faculty of Engineering of University of Porto). Cyclic loading experimental tests were carried out on rectangular hollow-section piers in order to study two main aspects: i) the influence of shear effects on the seismic response and, ii) the influence of transverse reinforcement details, in terms of cross section area with the correspondent effects on the shear capacity and concrete confinement. In addition, numerical simulations of the experimental tests were systematically carried out allowing complete and consistent interpretations of experimental results, for which the most important aspect was found associated with the shear influence on pier response. The adopted numerical methodology (Damage Model) allows realistic simulations of the non linear behavior, particularly when significant shear component is involved. In fact, shear deformation and also the shear mode failures were quite well simulated by this numerical strategy that also allowed identifying some relevant modeling issues that are likely to affect the quality of simulations.

KEYWORDS: Hollow-section bridge piers, shear failure, non-linear cyclic behavior, experimental tests, numerical simulations

1 INTRODUCTION

Hollow bridge piers generally have large section dimensions, with reinforcement bars spread along both wall faces. In addition, by contrast with common solid section columns, quite often the shear effect has great importance on the pier response and, therefore, transverse reinforcement details may assume a significant importance on the cyclic behavior for this kind of elements. Thus, it is of particular relevance that special attention is given to this issue when the assessment and retrofit of RC hollow section piers is envisaged.
Experimental evidence concerning this topic is relatively scarce, as just a few studies are reported in the literature, namely the large-scale tests on rectangular hollow piers carried out by Yeh *et al.* (2002) and Pinto et al. (2003) and, more recently, the reduced scale hollow section bridge piers tested by Pavese *et al.* (2004) and Calvi *et al.* (2005). In this framework, a testing campaign was developed in the Laboratory of Earthquake and Structural Engineering (LESE) of FEUP (Faculty of Engineering of Porto University), aiming at the experimental and numerical study of RC hollow section bridge piers under lateral cyclic loading with axial force. The experimental campaign activity was performed on reduced scale bridge piers, utilizing detailed instrumentation to evaluate shear effects, and it was complemented with refined FE simulations allowing for better interpretations of both global and local responses. In addition, more simplified analysis tools were also used to examine their capabilities and limitations in the simulation of pier cyclic behavior.
The present paper mainly focuses on the experimental assessment of the influence of stirrup contents and detailing. For that purpose, two hollow section piers were chosen with different stirrup area but equal arrangement (according to EC8) in order to present and analyze their experimental cyclic response and to compare them with detailed numerical simulations resorting to advanced tools.

2 EXPERIMENTAL CAMPAIGN

2.1 Testing setup

The setup shown in Fig. 1a was adopted in the experimental campaign. The system includes a 500 kN actuator to apply lateral loads with +/-100mm stroke and a 700 kN actuator to impose axial loads, using two reaction frames (lateral and vertical). Both the specimen and the reaction frames are bolted to the strong floor with high strength prestressed rods. In the tests described below, a constant axial load was applied while the lateral loading was cycled under displacement controlled conditions. Since the axial load remains in the same position while the specimen deflects, a special sliding device is used in order to minimize spurious friction effects. As shown in Fig. 1b, the device consists of two steel plates, the lower one bonded to the specimen top section and the top plate hinged to the vertical actuator, allowing top displacements and rotations on the specimen to occur when lateral loading is imposed. The upper plate is connected to a load cell reacting against the lateral frame in order to measure the residual frictional force between the two plates. This force is then subtracted to the horizontal actuator load, in order to obtain the correct force imposed to the specimen. The hydraulic system of the vertical actuator was designed to keep the oil pressure constant, thus ensuring a constant axial force during the tests. Data acquisition and signal conditioning cards provide direct readings from strain gauges, load cells and LVDTs (Linear Variable Displacement Transformer).

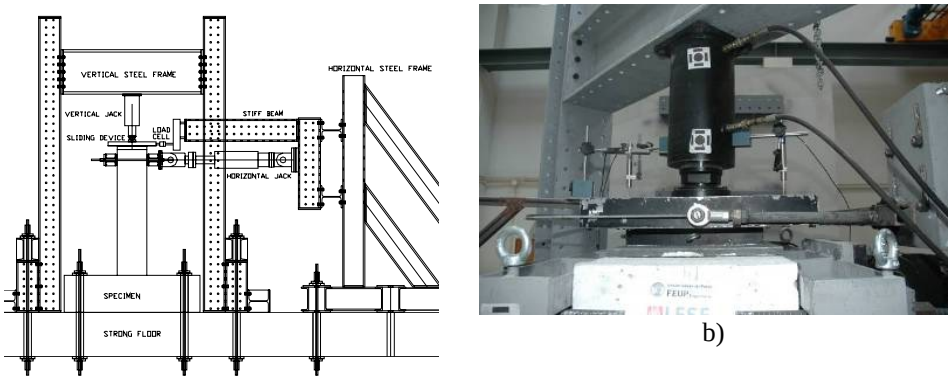

a) b)

Figure 1 Test setup at LESE laboratory: a) schematic layout and b) axial load sliding device.

2.2 Specimens and instrumentation

The specimens presented hereafter were based on similar ¼ scale models tested at the Laboratory of Pavia University, Italy (Calvi *et al.* (2005); Pavese *et al.* (2004)), in which only square sections were considered. The present study aimed at an extension of the Pavia tests, by introducing also a rectangular section type and different reinforcement details.

Therefore, out of the whole set of square and rectangular section models tested in this experimental campaign (fully described in Delgado (2008)), two model specimens were chosen to be presented in this paper. Fig. 2a shows these specimens that consist of rectangular hollow section RC piers with 450mm x 900mm external dimensions and 75mm thick walls, herein referred to as PO2.

Concrete composition was specifically studied, such that the maximum particle size did not exceed 10mm in order to be compatible with the specimen dimensions. The unconfined concrete compressive strength, measured on the day of the testing, was 28 MPa. The longitudinal reinforcement consisted on 8mm-diameter bars with 560 MPa yield strength, whereas stirrups were of 2.6mm plain bars with approximately 450 MPa yield strength and 190 GPa Young modulus. The transverse reinforcement details adopted for these piers comply with the EC8 provisions, as illustrated in Fig. 2a, and only differ on the area of transverse reinforcement, being the area of pier PO2-N6 the double of pier PO2-N5. Since important shear deformations were expected in these tests, an appropriate instrumentation configuration was adopted along the pier height using the LVDT layout shown in Fig. 2b for both specimen types, in order to allow measuring independently both the shear and flexural components of the specimen deformation.

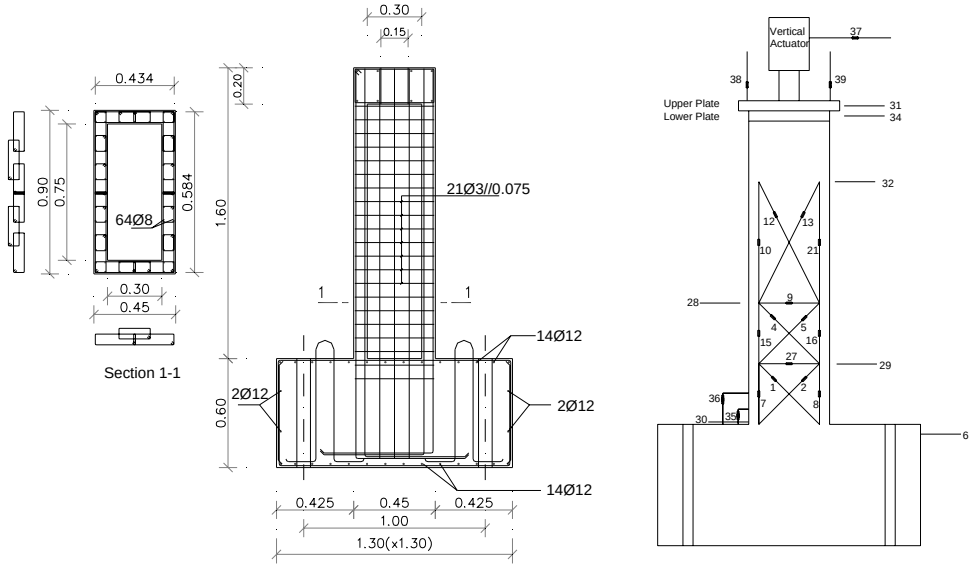

a) b)

Figure 2 Hollow RC piers: a) geometry of specimen and b) lateral LVDT layout.

2.3 Loading history

In order to characterize the cyclic behavior of both pier specimen (PO2-N5 and PO2-N6), three cycles were applied for each of the following peak displacements (mm): 1, 3, 5, 10, 4, 14, 17, 7, 25, 30, 33, 40, 45, under a constant axial load of 250 kN that corresponds to a normalized axial force of 0.08.
It is worth noting that these target displacements refer to measurements taken from the internal transducer of the hydraulic actuator that is affected by spurious deformations due to the reaction system and also to the rotation of the foundation. Since the actual specimen displacements do not match exactly those values, the correct values had to be obtained from an external transducer positioned at the level of the horizontal actuator axis, discounting the deflection due to foundation rotation that was also measured through a pair of vertical LVDTs located at the top part of the pier foundation. This implies that in each test displacements (and drifts) achieved by the specimen were not the same as those prescribed. Nevertheless, from the obtained force-displacement diagrams five deformation control stages were selected for the purpose of the analysis described below. These stages, labelled from D1 to D5, are listed in Table 1, together with the achieved net displacement and drift referring to the free pier height, i.e. 1.40m. These values may slightly differ from pier PO2-N5 to PO2-N6, and between positive and negative sense.

Table 1 Control stages for top-displacements and drifts during the tests

Control Stage	D1	D2	D3	D4	D5
Target Displ. (mm)	5	17	25	33	45
Achieved Displ. (mm)	3	13	20	30	44
Achieved Drift (%)	0.21	0.93	1.43	2.14	3.14

3 CYCLIC TESTS

The most relevant results obtained from the two tests (specimens PO2-N5 and PO2-N6), are reported hereafter. In the discussion, the North and South direction refer to the pier flange walls that are perpendicular to the loading direction whereas the East and West direction refer to the pier webs which are parallel to the loading. The top force- lateral displacement curves are depicted in Fig. 3.

From the cracking patterns shown in Figs. 4 and 5, it becomes clear that the pier webs were the most damaged zones of both specimens, exhibiting inclined cracking. On the other hand, the flange walls exhibited mainly horizontal cracking, except near the pier top region where inclined cracks also developed.
For both piers, the early test stages D1 were largely characterized by cracking near the pier base (approximately in the lower third of the height of the specimen), inclined in the webs and horizontal in the flanges, roughly spaced at 7.5cm and in correspondence with the stirrup spacing. This observation is in agreement with the force-displacement plots in Fig. 3, where the 0.21% drift line corresponds to the onset of cracking in both specimen tests.
Subsequent increasing of the displacement to stage D2 (0.93% drift) has induced generalized cracking along pier height, inclined at approximately 45º in the webs as shown in Figs. 4a and 5a, for PO2-N5 and PO2-N6, respectively. For this deflection level, the reference line in Fig. 3 confirms an advanced cracked behavior that developed close to the peak force. Internal damage was also monitored by video cameras as shown in Fig. 6, further evidencing wider cracking in the webs of pier PO2-N5 rather than in PO2-N6. For this stage, the North and South flanges exhibited crack widths not exceeding 0.3mm, a reduced damage state when compared with the damage in the webs. This observation indicates that shear deformations are dominant over the flexural components, notwithstanding the fact that shear effects are more controlled in PO2-N6 rather than in PO2-N5 due to the increase of transverse reinforcement in PO2-N6 (stirrup area is twice as much that of PO2-N5).

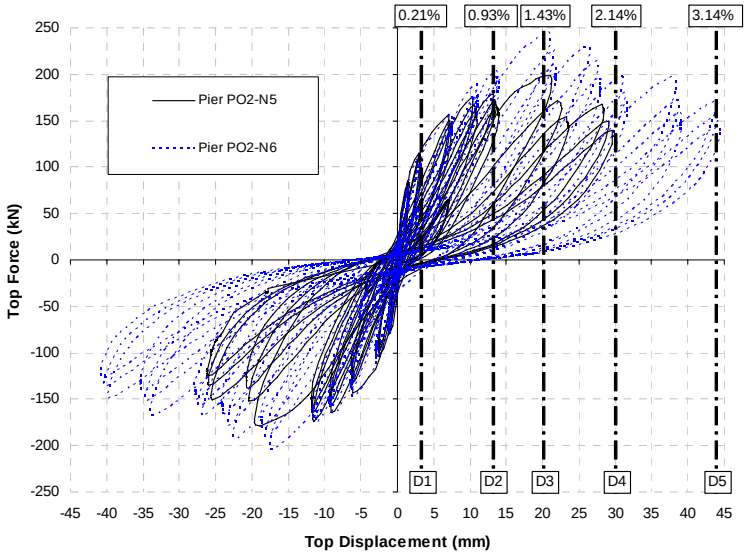

Figure 3 Experimental result comparison: PO2-N5 vs PO2-N6

At stage D3 (1.43% drift; 20mm deflection) further cracking developed in both piers with crack width of the order of 1.5mm (Figs. 4b and 5b) while concrete cover started spalling off in the webs of the PO2-N5 pier (but not for the PO2-N6). It is noteworthy that this drift level corresponds to the peak force reached during the test as evidenced by the reference line in Fig. 3, beyond which both piers entered the softening regime without any visible plastic plateau. This fact suggests once again that a shear strength mechanism seemed to prevail over the bending one, since no apparent exploitation of the bottom plastic hinge actually took place.
Cycling specimens at subsequent deformation levels resulted in a significant increase of damage (see Figs. 4c and 5c for stage D4, 2.14% drift, 30mm deflection) and, by the end of the tests, large portions of concrete cover spalled off in the webs and practically over the entire pier height. For PO2-N5 the test was stopped at stage D4, whereas for PO2-N6 it was pushed further up to stage D5 (3.14% drift, 44mm deflection) for which the damage state, as shown in Fig. 5d, is similar to that of PO2-N5 at the end of the test (Fig. 4c). Note that, at the final stage, low-to-moderate damage was observed in the North and South flanges, but cracks were no more exclusively horizontal, as usual for T- or I-shaped sections, due to the so-called “shear lag effect” that occurs for the ratio flange-width/section-height of about 2:1 or above, as in the present specimen case.

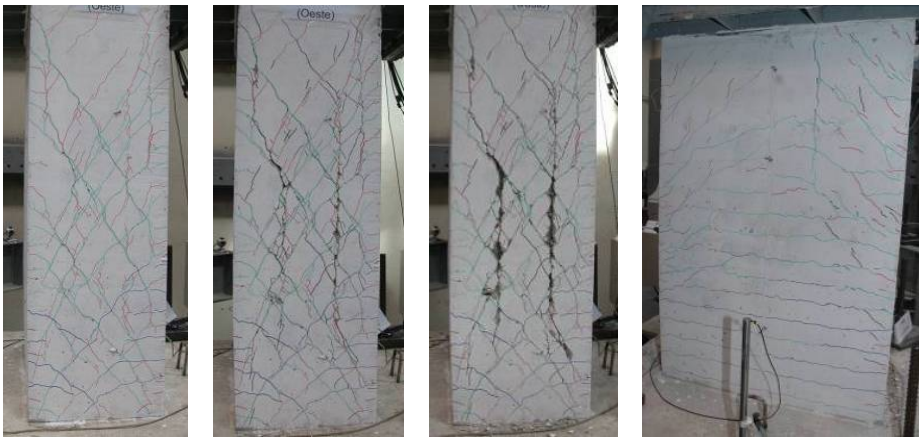

(a) 0.93% drift (West) (b) 1.43% drift (West) (c) 2.14% drift (West) (d) 2.14% drift (North)

Figure 4 Pier PO2-N5: external damage evolution

(a) 0.93% drift (West) (b) 1.43% drift (West) (c) 2.14% drift (West) (d) 3.14% drift (West)

Figure 5 Pier PO2-N6: external damage evolution

a) b)

Figure 6 Internal damage in the West web for 0.93% drift: a) PO2-N5 and b) PO2-N6

Regarding strength, it is clear that specimen PO2-N6 performed better, leading to a peak force 20% larger than for PO2-N5 at the same deflection level (stage D3, at 1.43% drift). According to the above, significant damage related with shear deformations was observed in the web walls causing pronounced degradation of concrete. This effect was also visible in PO2-N6, but it was more evident and anticipated for pier PO2-N5. In terms of force-displacement response, this is reflected in the reduction of the restoring force during the 3-cycle set at each drift level and is associated to the stiffness degradation introduced by shear cracking. In fact, due to cracking induced in the 1st cycle, shear deformations increase in the 2nd and 3rd cycles thus amounting to a larger contribution for the total imposed displacements. Consequently, the corresponding bending component of the deflection becomes lower, entailing also a reduction of force demands in the referred cycles.

The relative amount of shear and bending deformations in these tests is an important matter that deserves further attention. Therefore, resorting to instrumentation readings concerning horizontal displacements at several elevation levels as well as the top and base section rotations, it was possible to estimate the flexural component of the deformation. This was performed by assuming a cubic deflected shape consistent with an equivalent average bending stiffness (EI)eq (where E is the Young modulus and I is the moment of inertia) that allows writing an expression for the top section rotation. Since this rotation was measured and the bending moment diagram is known, the rotation profile can be obtained by curvature integration (thus, integration of moments), taking as boundary conditions the measured top section rotation and null rotation at the base (as mentioned before, the foundation rotation was discounted from the displacements measured by external transducers). This procedure allows estimating the (EI)eq value as well as another integration constant. Further integration leads to the desired bending displacement profile, by imposing null displacement at the base section.
Following this process, the charts shown in Fig. 7 (a and b) were drawn where the relative contributions of shear and bending deformation components are expressed for the 1st cycle peak of each achieved displacement on both pier specimens. In Fig 7c the bending (B) and total (T) displacement profile is illustrated for both piers at stage D3, which corresponds to 20mm top displacement.
It is clear that the shear component is more important for PO2-N5 than for PO2-N6, particularly in the larger amplitude cycles where more degradation is observed due to shear cracking. In fact, it is clear that in pier PO2-N6, with twice the stirrup area than in specimen PO2-N5, the shear deformation component is better controlled and leads to an increased bending component for the imposed displacement, with larger extensions in the longitudinal bars, associated with higher horizontal forces as already described.

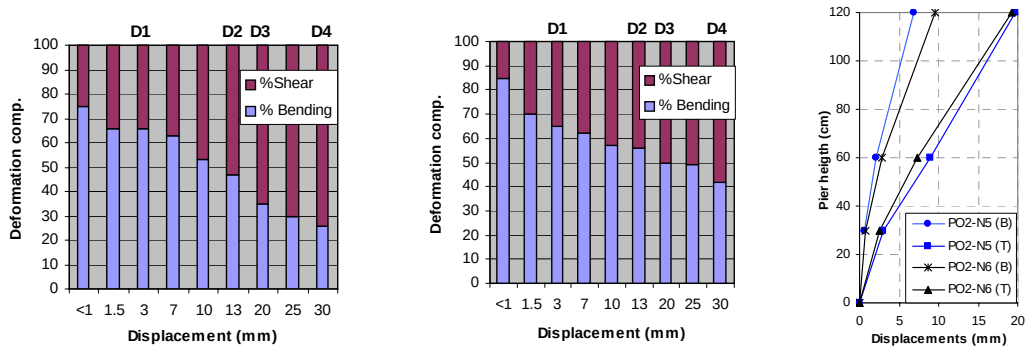

a) PO2-N5 b) PO2-N6 c) deformed shape for D3

Figure 7 Shear and bending deformation components and displacement profiles, c), for piers PO2-N5 and PO2-N6

A final comment should be made concerning the non-symmetry of the cyclic response for positive and negative bending, as visible in Fig. 3, where larger restoring forces were recorded in the positive direction. This non-symmetry is partially justified by the different displacements that developed in the two directions leading to less restoring force in the negative direction where lower displacements were actually imposed for each target displacement set. In any case, this effect is also associated with the shear cracking extension and reversal process. Once a set of cracks is open for a given loading sense, the reversal into the opposite sense is partially done by closing of the previously opened shear cracks. Therefore, as the shear stiffness component decreases, for a given horizontal displacement imposed, the displacement component due to bending effect becomes lower thus mobilizing lower restoring forces. After the peak force, these effects are even more evident due to the use of plain steel bars, responsible for very poor concrete-steel bond conditions and, consequently, leading to more pronounced and wide cracks.

4 NUMERICAL ANALYSIS

Numerical analysis for cyclic loading were carried out with the CAST3M computer code, CEA (2003), a general purpose finite element based program, where a wide variety of non-linear behaviour models are available. In particular, the damage model developed at FEUP (Faria *et al.* (1998)), is also implemented in CAST3M (Costa *et al.* (2005)) and has already proved to be suitable for seismic behaviour analysis of RC bridge piers as shown by Faria *et al.* (2004). More recently it has been also adopted by Delgado *et al.* (2007) for numerical simulation of piers within the experimental campaign referred herein. Therefore, the present

modelling approach involves the above mentioned Continuum Damage Mechanics-based constitutive model for the concrete zone discretized with 3D finite elements, incorporating two independent scalar damage variables that account for the degradation induced by tensile or compressive stress conditions. The Giuffré-Menegotto-Pinto model, Giuffrè et al. (1970), also available in CAST3M, is used for the simulation of the cyclic behaviour of the steel reinforcement which is discretized via truss elements.
Results of the numerical model for pier PO2-N5 and PO2-N6 are included in Fig. 8, where the global response is compared with experimental results. As referred above, shear deformation/failure mechanisms were observed on both piers' response from early test stages. These effects were satisfactorily simulated by the numerical damage model, leading to values of peak force within less that 15% from those recorded during the tests.

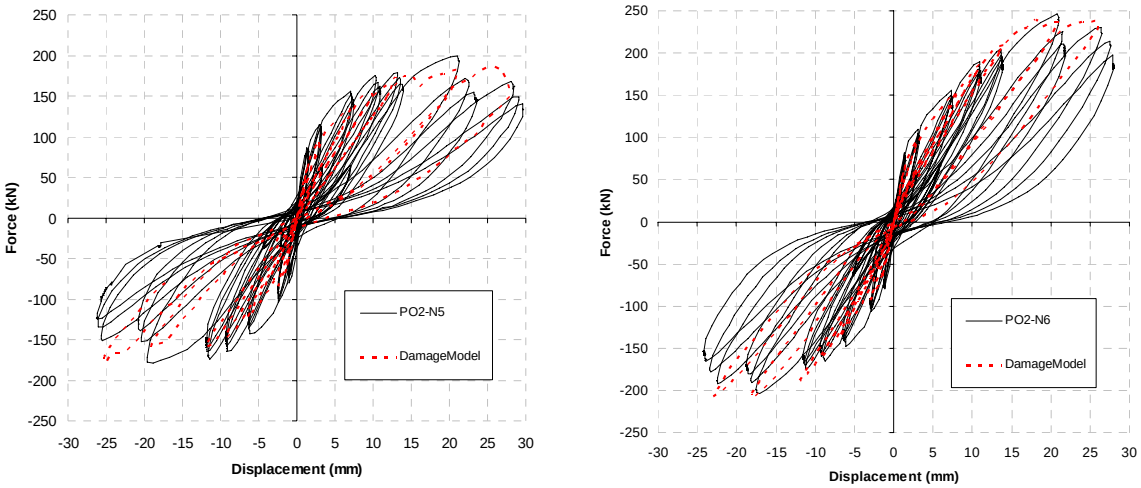

a) Pier PO2-N5 b) Pier PO2-N6

Figure 8 Comparison of experimental and numerical results

The results of the numerical model, for the horizontal displacement of 20mm (1.43% drift), showed that the deformed mesh of pier PO2-N5 seems to exhibit larger contribution of shear deformation (Fig. 9a) than pier PO2-N6 (Fig. 9c), thus confirming some of the conclusions stated before in this paper. For this displacement level the shear component takes a significant importance on the pier behavior and is even responsible for the collapse mechanism, as reflected by stirrup yielding along the entire pier high. In fact, the transverse reinforcement stress pattern from the numerical model allowed identifying the development of strut-and-tie shear mechanisms with extensive yielding of stirrups.

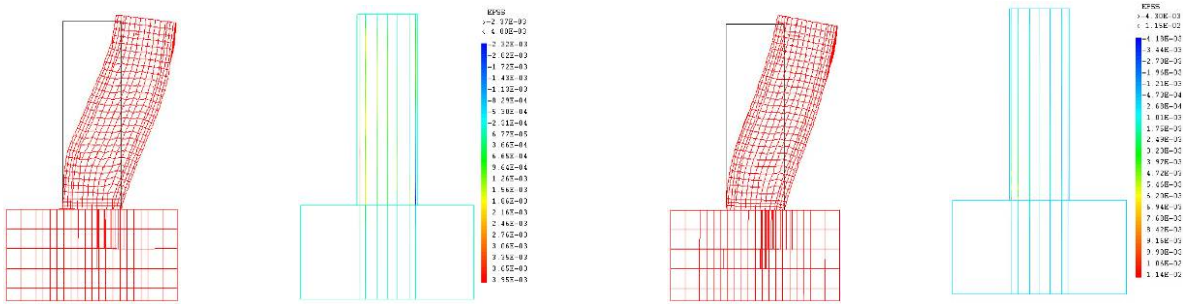

a) Deformed mesh (PO2-N5) b) Longitudinal reinf. strain (PO2-N5) c) Deformed mesh (PO2-N6) d) Longitudinal reinf. strain (PO2-N6)

Figure 9 Numerical results at stage D3 (1.43% drift; d = 20mm)

In addition, from the results shown in Figs. 9b and 9d, for PO2-N5 and PO2-N6, respectively, at stage D3 (1.43% drift), it is possible to determine the strain distribution along the longitudinal reinforcing bars where steel yielding can be found. For the pier PO2-N5 these diagrams show the spread of strain distribution on the outer longitudinal bars caused by predominant shear deformation that is associated with lower rotation of the pier base region. In contrast, in pier PO2-N6 the inelastic strain is mainly concentrated in the outer bars right above the foundation, as a result of a larger bending contribution.

5 CONCLUSIONS

Although the collapse of the two piers presented in this paper was caused by shear mechanisms, the experimental results allow concluding that the pier with double transverse reinforcement (PO2-N6) resisted 20% more in terms of peak load and reached a displacement about 50% larger in comparison with specimen PO2-N5, for a similar residual force. Furthermore, results of pier PO2-N6 shown a decrease of the shear deformation component, as experimentally confirmed by the larger flexural component recorded. However, since the failure was triggered by shear, this study was not yet conclusive for evaluating the efficiency of EC8 transverse reinforcement detailing to prevent buckling of longitudinal bars, being carried out more tests in order to make that evaluation after shear retrofitting of these piers. On the other hand, this double area transverse reinforcement was found to contribute for the reduction of shear crack opening in the pier web walls, thus leading to lower concrete damage. The numerical modelling strategy, which involved a detailed representation of the concrete and steel behavior, allowed capturing the main issues of the global cyclic response as obtained by the experimental tests. The numerical results were in fairly good agreement with those recorded during the tests, both in terms of the peak restoring force and the global pier stiffness. The numerical analysis also confirmed the experimentally observed shear failure, being this type of advanced numerical modelling, which allow for the representation of non linear shear effects, an important and valuable insight on hollow piers behavior, mainly, when important shear deformations are involved.

ACKNOWLEDGEMENTS

The authors wish to acknowledge the “Irmãos Maia, Lda” company, for the construction of the tested piers. Final acknowledgements to the laboratory staff, mainly Mr. Valdemar Luís, for all the care on the test preparation. This study was performed with the financial support of the “FCT- Fundação para a Ciência e Tecnologia" through the Project PTDC/ECM/72596/2006, ”Seismic Safety Assessment and Retrofitting of Bridges”.

REFERENCES

Calvi GM, Pavese A, Rasulo A, Bolognini D (2005) Experimental and numerical studies on the seismic response of R.C. hollow bridge piers. *Bulletin of Earthquake Engineering*, **3 (3)**: 267-297

CEA (2003) Pasquet P. Manuel d’utilisation de Cast3m, Commissariat à l’Énergie Atomique

Costa C, Pegon P, Arêde A, Castro J (2005) Implementation of the Damage model in Tension and Compression with Plasticity in Cast3m. Report EUR, ISPC, CEC, JRC, Ispra (VA), Itália

Delgado P, Rocha P, Pedrosa J, Arêde A, Pouca, NV, Santos M, Costa A, Delgado, R (2007) Retrofitting of Bridge Hollow Piers with CFRP. Paper presented at the Thematic Conference on Computational Methods in Structural Dynamics and Earthquake Engineering. Crete, Greece, 13-16 June 2007

Delgado P (2008) Avaliação da Segurança Estrutural em Pontes. PhD Thesis, FEUP, Porto (in Portuguese)

Faria R, Oliver J, Cervera M (1998) A strain based plastic viscous damage model for massive concrete structures. *International Journal of Solids and Structures*, **35 (14)**: 1533-1558

Faria R, Pouca NV, Delgado R (2004) Simulation of the Cyclic Behaviour of R/C Rectangular Hollow Section Bridge Piers via a Detailed Numerical Model. *Journal of Earthquake Engineering*, **8 (5)**: 725-748

Giuffrè A, Pinto P (1970) Il comportamento del cemento armato per sollecitazione ciclice di forte intensitá. Giornale del Genio Civile

Pavese A, Bolognini D, Peloso S (2004) FRP seismic retrofit of RC square hollow section bridge piers. *Journal of Earthquake Engineering*, **8 (1 SPEC. ISS.)**: 225-250

Pinto AV, Molina J, Tsionis G (2003) Cyclic tests on large-scale models of existing bridge piers with rectangular hollow cross-section. *Earthquake Engineering and Structural Dynamics*, **32 (13)**: 1995-2012

Yeh YK, Mo YL, Yang CY (2002) Full-scale tests on rectangular hollow bridge piers. *Materials and Structures*, **34 (246)**: 117-125